Gyrokinetic Studies of Turbulence, Equilibrium, and Flows in the Tokamak Edge

B. D. Scott[1], F. Da Silva[2], A. Kendl[3], N. Miyato[4], T. Ribeiro[1,2]

[1]Max-Planck-Institut für Plasmaphysik, EURATOM Association, D-85748 Garching
[2]Instituto de Plasmas e Fusão Nuclear, Euratom, Lisbon, Portugal
[3]Inst fuer theor Physik, Euratom/OeAW, University of Innsbruck, Innsbruck, Austria
[4]Japan Atomic Energy Agency, Naka, Ibaraki, Japan
e-mail: bruce.scott@ipp.mpg.de

Abstract. We report on developments in the theory and computation of gyrokinetic turbulence in the tokamak edge. A new formulation of the gyrokinetic Lagrangian for the strong ExB-flow regime is been found, with clear correspondence to previous forms and to reduced MHD. Conservation of energy, momentum, entropy, and particles is demonstrated at both theoretical and computational level. Neoclassical phenomena and MHD equilibration are shown in our electromagnetic total-f phase-space computational model FEFI. Delta-f gyrokinetic edge turbulence is computed on the full flux surface with the local fluxtube model delta-FEFI and results on the edge/core transition are given. We also present ongoing gyrofluid studies of ELM crash scenarios, including the influence of the bootstrap current in an edge pedestal model on both the initial instability and the resulting turbulence. These studies and findings are centrally relevant to further understanding of the H-mode and pressure profile pedestal in large tokamaks.

1. Electromagnetic Gyrokinetic Theory

In the context of gyrokinetic field theory [1–3], a new formulation of the gyrokinetic Lagrangian for the situation of low beta and strong ExB flow was given in Ref. [4]. Generally there are two ways to obtain a gyrokinetic Lagrangian via Lie transforms: the field variable amplitude is small but the scale of motion is arbitrary, or the scale of motion is large compared to the gyroradii of all species and the field variable amplitude is arbitrary. These are the approaches of Refs. [5,6] or [7], respectively. Our method follows the mathematics of Ref. [7] but with two changes: first the large scale flow is determined by the Euler-Lagrange equations at zeroth order to be the ExB flow, as in Ref. [8], and not an arbitrary background flow given by a fluid analysis. Secondly, the strategy of Ref. [6] explicitly using the transform gauge freedom to arrange all effects of the dependent variables into the Hamiltonian. Therefore, the single variable covers both equilibrium and fluctuating flows, and no field-variable time derivatives explicitly appear in the equations. This is the maximal benefit for computations. We also obtain the added benefit of direct proof of correspondence to the Ref. [6] form in his long-wave and our small-amplitude limit, and also very naturally to nonlinear reduced MHD. These demonstrations are given in Ref. [4].

In limit $\mathbf{v}_E \ll c_s$ (subsonic ExB flow) the electrostatic Lagrangian of Ref. [4] reduces to the low-$k_\perp$ (small perpendicular wavenumber, hence long-wave) limit of Ref. [6]. Electromagnetic extension using the canonical parallel momentum as a (gyrocenter) particle coordinate is straightforward. The particle coordinates are $\mathbf{Z}_p = \{\mathbf{R}, p_z, \mu, \vartheta\}$, the gyrocenter position, canonical parallel momentum, generalised magnetic moment, and gyrophase angle, with ϑ ignorable and μ an adiabatic invariant to second order (the order kept) in the expansion parameter m/e. All appearance of the dependent field variables $\{\phi, A_\parallel\}$ is stricly arranged into the time component. In the subsonic, low-beta electromagnetic limit ($\beta_e = \mu_0 p_e/B^2 \ll 1$), the particle Lagrangian and Hamiltonian are

$$L_p = (e\mathbf{A} + p_z\mathbf{b})\cdot\dot{\mathbf{R}} + \frac{m}{e}\mu\dot{\vartheta} - H \qquad H = m\frac{U^2}{2} + \mu B + e\phi_G \tag{1}$$

respectively, where

$$U \equiv \frac{\partial H}{\partial p_z} = \frac{p_z}{m} - \frac{e}{m} J_0 A_\parallel \qquad \phi_G = J_0\phi - \frac{e}{2B}\frac{\partial}{\partial \mu}\left[J_0(\phi^2) - (J_0\phi)^2\right] \tag{2}$$

are functions of the coordinates. The drift component of the Euler-Lagrange equations is

$$B_\parallel^* \frac{d\mathbf{R}}{dt} = \nabla H \cdot \frac{\mathbf{F}}{eB} + U\mathbf{B}^* \qquad B_\parallel^* \frac{dp_z}{dt} = -\mathbf{B}^* \cdot \nabla H \tag{3}$$

separating naturally from the gyromotion given by $d\mu/dt = 0$ and $d\vartheta/dt = (e/m)\partial H/\partial\mu$. The other quantities

$$\mathbf{A}^* = \mathbf{A} + \frac{p_z}{e}\mathbf{b} \qquad \mathbf{B}^* = \nabla\times\mathbf{A}^* \qquad B_\parallel^* = \mathbf{b}\cdot\mathbf{B}^* \qquad \mathbf{F} = \nabla\mathbf{A} - (\nabla\mathbf{A})^T = \varepsilon\cdot\mathbf{B} \tag{4}$$

are functions of the geometry. The superscript T denoting the transpose, and ε is the rank-three Levi-Civita pseudotensor. It follows that $\nabla\times\mathbf{b} = -\nabla\cdot(\mathbf{F}/B)$ and $\mathbf{B}^* = \mathbf{B} - p_z\nabla\cdot(\mathbf{F}/eB)$.

The system Lagrangian is constructed by embedding particles in a phase space and then using a continuous distribution function in that space with the relationships between particle coordinates and phase space independent variables understood. The phase space volume element is

$$d\Lambda = dV \otimes dW \qquad dV = \sqrt{g}\,dx^1\,dx^2\,dx^3 \qquad dW = 2\pi m^{-2}\,dp_z\,d\mu\,B_\parallel^* \tag{5}$$

where $\sqrt{g}$ is the determinant of covariant components of the coordinate metric. The system Lagrangian is

$$L = \sum_z \int d\Lambda\, f L_p - \int dV\, \frac{B_\perp^2}{2\mu_0} \qquad B_\perp^2 = \left|\nabla_\perp A_\parallel\right|^2 \tag{6}$$

where the sum is over species and the field term is the contribution due to magnetic field energy. There is no electric field energy term because the assumption of quasineutrality has been taken.

The equations of motion consist of the gyrokinetic equation for f and field equations for the potentials ϕ and $A_\parallel$. The gyrokinetic equation may be case in the antisymmetric bracket form

$$\frac{\partial f}{\partial t} + \mathcal{E}^{abcd} H_{,a} f_{,b} A^*_{c,d} = 0 \tag{7}$$

where $\mathcal{E}$ is the rank-four Levi-Civita pseudotensor in the 4-space covered by $dV \otimes dp_z$. The components of $\mathcal{E}^{abcd}$ are $1/\sqrt{g}B_\parallel^*$ times ± 1 or 0 depending on the permutation of indices $\{abcd\}$ in the 4-space domain. The 3-space order is $\{123\}$ for $dx^1\,dx^2\,dx^3$ and hence the 4-space order is $\{123z\}$ for $dx^1\,dx^2\,dx^3\,dp_z$. Positive, negative, and zero permutations of these give the other components. The gyrokinetic Poisson and Ampere equations for this system are found by setting the functional derivative of L with respect to ϕ or $A_\parallel$ respectively to zero,

$$\sum_z \int dW\,[eJ_0 f + \{J_0\mathcal{M}J_0 - (J_0\mathcal{M})\}\phi] = 0 \qquad \nabla_\perp^2 A_\parallel = -\mu_0 \sum_z \int dW e J_0(fU) \tag{8}$$

where $\mathcal{M} \equiv -(e^2/B)\partial f/\partial\mu$ defines the polarisability (for a Maxwellian, $\mathcal{M} = e^2F^M/T$).

The particle canonical toroidal momentum is given by the toroidal covariant component of $\mathbf{A}^*$, via $P_\varphi = eA_\varphi^*$. For a tokamak magnetic geometry with $\mathbf{B} = I\nabla\varphi + \nabla\psi\times\nabla\varphi$ we have $A_\varphi^* = \psi + (I/eB)p_z$ The corresponding phase space continuity equation is

$$\frac{\partial}{\partial t}(fP_\varphi) + \frac{1}{\sqrt{g}B_\parallel^*}\frac{\partial}{\partial \mathbf{Z}_p}\cdot(\sqrt{g}B_\parallel^* f P_\varphi \dot{\mathbf{Z}}_\mathbf{p}) = -f\frac{\partial H}{\partial\varphi} \tag{9}$$

Similarly, the corresponding form for energy is

$$\frac{\partial}{\partial t}(fH)+\frac{1}{\sqrt{g}B_{\|}^{*}}\frac{\partial}{\partial \mathbf{Z}_{p}}\cdot(\sqrt{g}B_{\|}^{*}fH\dot{\mathbf{Z}}_{\mathbf{p}})=f\frac{\partial H}{\partial t} \tag{10}$$

These forms are valid for any dependence of H upon the field variables, so long as these do not appear in the symplectic part of L (the part dependent upon the time derivatives of the particle coordinates). It is vital to have Lie-transformed ϕ and $A_{\|}$ into H following the strategy of Ref. [4]. In a recent preprint [9], we have proved, using the vorticity continuity equation, that for any H the momentum conservation equation is

$$\frac{\partial}{\partial t}\left\langle -\mathbf{P}\cdot\nabla A_{\varphi}\right\rangle+\frac{\partial}{\partial t}\left\langle fp_{z}b_{\varphi}\right\rangle+\frac{\partial}{\partial V}\left\langle fp_{z}b_{\varphi}\dot{V}\right\rangle+\left\langle f\frac{\partial H}{\partial \varphi}\right\rangle=0 \tag{11}$$

where $\nabla\cdot\mathbf{P}=\sum_{z}\int dW\,fe$ defines the polarisation vector. The generalised vorticity is $-(1/n_{e}e)\nabla\cdot\mathbf{P}$, which reduces to the usual $B_{0}^{-1}\nabla_{\perp}^{2}\phi$ form in the limit of delta-f reduced MHD. For H dependent upon $\{\phi,A_{\|},\nabla\phi,\nabla A_{\|}\}$ the last term Eq. (11) becomes

$$\left\langle f\frac{\partial H}{\partial \varphi}\right\rangle=\frac{\partial}{\partial V}\left\langle\frac{\partial\phi}{\partial\varphi}\nabla V\cdot f\frac{\partial H}{\partial\nabla\phi}\right\rangle+\frac{\partial}{\partial V}\left\langle\frac{\partial A_{\|}}{\partial\varphi}\nabla V\cdot\left(f\frac{\partial H}{\partial\nabla A_{\|}}+\frac{1}{\mu_{0}}\nabla_{\perp}A_{\|}\right)\right\rangle \tag{12}$$

The term involving $\mathbf{P}$ is identified as the ExB component of the toroidal momentum by illustrating the results in the MHD limit (cf. Ref. [4] for details). The terms in Eq. (12) give the field-field Reynolds and Maxwell stresses, respectively. All of these forms are obtained under any ordering in the Lie-transform. They are underlain by exact energetic consistency, in which approximation is restricted to the establishment of H,L_{p},L and after that all reductions are rigorous. In much of the current discussion the field theoretical underpinnings, let alone energetic consistency, are usually not discussed even if barely mentioned at all.

2. Electromagnetic Gyrokinetic Computation

Computational models for the total-f form given by the above Lagrangian (Eq. 6) and its delta-f limit are called FEFI [10] and delta-FEFI [11], respectively. Stricty energetic consistency is obtained in the delta-f limit (not the delta-f computational method for a total-f equation, by contrast) only if the geometry and equations are put into the local fluxtube limit. FEFI is still under development and axisymmetric flow/current cases have been managed. Delta-FEFI is mature and has obtained several results for core and edge turbulence cases; however, it cannot become a global model. Eventually, fluxtube models are useful for studies of intrinsic physics but the edge eventually requires a total-f model. The status of these is given below.

2.1. Total-F Axisymmetric Cases

In general either global or local versions are best done in flux coordinates to avoid problems with large components of the nonlinear parallel gradient in the radial direction on the computational grid. True field aligning is only relevant to turbulence; for axisymmetric cases, any system of flux coordinates is automatically field aligned (the undisturbed parallel gradient involves the poloidal coordinate only). The arrangement of the gyrokinetic equation as in Eq. (7) allows simple replacement of any flux coordinate system by any other in the computations. Unfortunately, the MHD equilibrium is a result; only its approximation is an input. Dynamical flux surface following by the grid is still under development. Until then we must face radial components in $\nabla_{\|}$ (given by the pieces with d poloidal and b radial in the indices in Eq. 7).

At the moment FEFI is using the low-$k_\perp$ version of the above Lagrangian, with

$$U \quad \rightarrow \quad \frac{p_z}{m} - \frac{e}{m}A_\parallel \qquad\qquad \phi_G \quad \rightarrow \quad \phi - \frac{m}{2eB^2}\left|\nabla_\perp \phi\right|^2 \tag{13}$$

thereby concentrating upon equilibrium phenomena. The short-term aim is benckmark against theory and other codes for neoclassical bootstrap flows and currents. In Ref. [10] the control case was given: in the absence of collisions there are no such bootstrap phenomena, and the radial electric field relaxes to a close approximation of static radial force balance for the ions: $ne\phi_{,x} + p_{,x} \approx 0$ for a single-species case with singly charged ions, where x denotes the radial component, and n and p are the computed density and pressure moments of f, respectively.

Herein, we add collisions, so that Eq. (7) becomes

$$\frac{\partial f}{\partial t} + \mathcal{E}^{abcd} H_{,a} f_{,b} A^*_{c,d} = C(f) \tag{14}$$

where the collision operator C is a combination of like-like pitch-angle and energy scattering for each species plus electron-ion pitch-angle scattering off each ion species. The like-like operator is formulated to conserve energy and momentum. True energy scattering is replaced by parallel-velocity diffusion due to problems at zero velocity in the implementation. The like-like operator is given by

$$C_z = \frac{\partial}{\partial \zeta}\nu_{zp}\frac{1-\zeta^2}{v^3}\frac{\partial}{\partial \zeta} - \frac{\partial}{\partial U}\nu_{ze}\left[(z-\alpha_z) - \beta_z \frac{\partial}{\partial U}\right] \tag{15}$$

where v and ζ are given by $v^2 = U^2 + 2\mu B$ and $\zeta = (U - \gamma_z)/v$ with U given in Eq. (2), and $\alpha_z, \beta_z, \gamma_z$ are parameters decided at each step to conserve energy and momentum by each part of C_z. In addition, the electron-ion pitch-angle scattering operator for each ion species is given by

$$C_e = \sum_i \frac{\partial}{\partial \zeta}\nu_{ei}\frac{1-\zeta^2}{v^3}\frac{\partial}{\partial \zeta} \tag{16}$$

with $\zeta = U/v$ simply. Then, for each ion species $C = C_z$ and for electrons $C = C_z + C_e$. The coefficients are 1.87997 times the Braginskii collision frequency for each species.

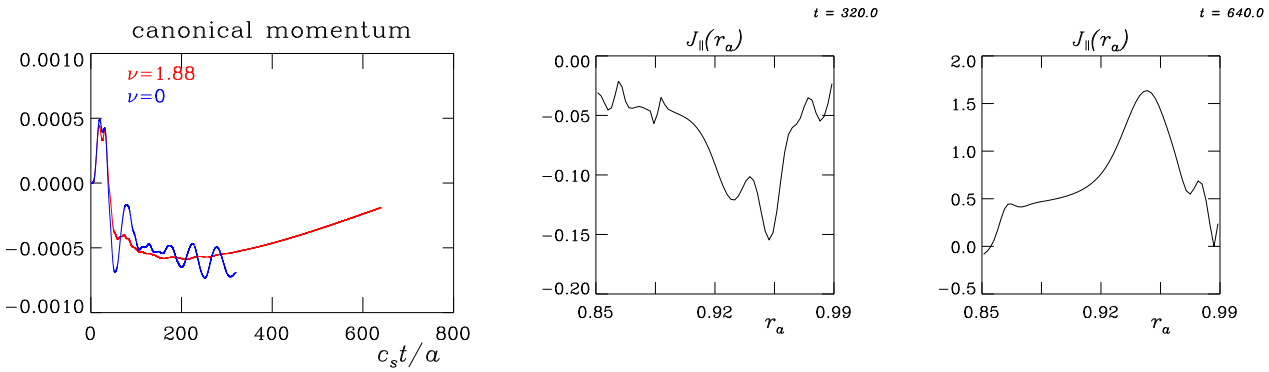

FIG. 1: Momentum conservation and zonal $J_\parallel$ profiles for FEFI, with ($\nu = \nu_e a/c_s$) and without collisions, the control test for bootstrap current. The value $\nu = 1.88$ is evaluated at nominal parameters (see text).

At this stage we demonstrate the presence/absence test of collisions on the bootstrap current. In Ref. [10] the collisionless control case gave the expected Pfirsch-Schlüter current $\cos\theta$ side-bands but negligible zonal current or zonal parallel flow. The details of the case are cited there;

nominal parameters refer to the mid-pedestal values of $T = 200\,\mathrm{eV}$ and $n = 2\times10^{19}\,\mathrm{m}^{-3}$, along with $R_0 = 3.3a = 1/65\,\mathrm{m}$ and $B = 2.5\,\mathrm{T}$. In the collisional case, a substantial bootstrap current in roughly the expected amplitude is found, corresponding to a drift velocity $J_\parallel/n_e e$ about 1.5 times the sound speed at the mid-pedestal radius. The collisions have no overall effect on momentum conservation. Further study will focus upon comparison to both neoclassical theory and experimental observations of toroidal flows.

2.2. Delta-F Fluxtube Turbulence Cases

The delta-f fluxtube model derived from the above, called delta-FEFI (dFEFI), is part of the derivation chain which ends in delta-f gyrofluid equations [11], which are the same as the GEM model of Ref. [12]. The polarisation and parallel dynamics are linearised except for the presence of the $\widetilde{A}_\parallel$ fluctuation in H to first order. This magnetic flutter nonlinearity then combines with the ExB one due to the $\widetilde{\phi}$ fluctuation. The linearisation of parallel dynamics forces use of a delta-f free energy rather than the total-f energy — as a result, the use of fluxtube geometric assumptions as well is mandatory, as explained in Ref. [11]. The model may be used for intrinsic turbulence studies as in conventional fluxtube modelling, but nonlocal phenomena are not treated. Nevertheless, well defined studies of turbulence character and enegetics are possible, and until the total-f efforts mature this is the best we have.

The model is defined by the delta-f gyrokinetic equation

$$\frac{\partial g}{\partial t} + \frac{F^{xy}}{eB^2}[H_1, h+f_0]_{xy} + \frac{B^s}{B}[H_0,h]_{zs} = \frac{mv_\parallel^2+\mu B}{2e}\mathcal{K}(h) + C(\delta f) \tag{17}$$

and the self consistent polarisation and induction equations

$$\sum_z \int dW\left[eJ_0(\delta f) + e^2F_0'(J_0^2-1)\widetilde{\phi}\right] = 0 \qquad \nabla_\perp^2 A_\parallel + \mu_0\sum_z\int dW\left[ev_\parallel J_0(\delta f)\right] = 0 \tag{18}$$

for the dependent variables δf, $\widetilde{\phi}$, and $A_\parallel$, where

$$H_0 = m\frac{v_\parallel^2}{2} + \mu B \qquad H_1 = eJ_o(\widetilde{\phi}) - ev_\parallel J_0(\widetilde{A}_\parallel) \qquad h = \delta f + F_0' eJ_0(\widetilde{\phi}) \qquad g = h - F_0' H_1 \tag{19}$$

$$F_0 = F^M(n,T) \qquad F_0' = \frac{F^M}{T} \qquad f_0 = F^M\left[\frac{1}{L_n} + \left(\frac{mv_\parallel^2}{T} - \frac{3}{2}\right)\frac{1}{L_T}\right](-x) \tag{20}$$

and the collision operator C is given by pitch angle scattering off a background (the C_{ei} piece from FEFI).

Each species is defined by mass m, charge e, and background density and temperature n, T. The 0th and 1st order pieces in H are H_0 and H_1 where $v_\parallel$ and μ are coordinates in $dW = 2\pi m^{-1}\,dv_\parallel\,d\mu\,B$. The background F_0 is the species Maxwellian F^M, and L_n and L_T are the species density and temperature gradient scale lengths.

Fluxtube geometry with perpendicular and parallel coordinates $\{xy\}\otimes s$ is defined by the drift tensor component F^{xy}, magnetic field strength B, poloidal/parallel component B^s, curvature operator $\mathcal{K}$, and metric coefficients g^{xx}, g^{xy}, g^{yy} using Hamada coordinates for which F^{xy}/B^2, B^s, and $\sqrt{g}$ are flux functions, with all details and derivations in Refs. [13,14]. Subscripted brackets such as $[a,b]_{xy}$ denote a Poisson bracket between the two quantities a, b in the given coordinate plane $\{xy\}$ The grid is in the coordinate space of $\{xys\}\otimes\{zw\}$ with the latter two covering $v_\parallel$ and μ in units of $V = \sqrt{T/m}$ and T/B_0.

The way in which edge turbulence cases are set up follows previous gyrofluid usage. Parameters are taken from a given point on the profile (in normalised volume minor radius r_a). The radial domain size L_x is limited by the local value of $L_\perp$ (the scale length of the steepest gradient — see Ref. [15] for the explanations of this and other local parameters). The drift angle is limited by the extent of perpendicular variation on the entire flux surface; in a circular model with minor radius a this is $L_y = 2\pi r/q$ with $r = r_a a$. For edge cases $L_y/L_x \gg 10$ leading to a strongly anisotropic longwave component. For typical L-mode cases with $T_e \sim 100\,\mathrm{eV}$ and $B = 2.5\,\mathrm{T}$ (cf. Ref. [16]) $L_x \sim 60\rho_s$ while $L_y \sim 1500\rho_s$ in units of the ion sound gyroradius (drift scale) ρ_s. The scale range $0.1 < k_y\rho_s < 1$ is the drift wave component, while $k_y\rho_s < 0.1$ is mesoscale MHD which is excited by both inverse ExB energy transfer and resonance with geodesic acoustic oscillations. The strength of the MHD component ultimately demands full flux surface computations even for a fluxtube model, which are presented herein. At the moment, only a scan in β_e is available; at the conference scans in collisionality $\nu_e L_\perp/c_s$ and shear $S = d\log q/d\log r$ as well as background ExB shear $\Omega_E = B_0^{-1} d^2\phi_0/d^2 r$ will be given. A zonal flow energetics study is also planned, pending operational serviceability of computational platforms.

2.3. Full Flux Surface Beta Scan

The basic result of any edge turbulence model is scaling of average turbulent fluxes in the deeply saturated regime, defined by the temporal stationarity in a statistical sense of all energy transfer channels. The parallel ion velocity fluctuations are usually the last element to saturate, so the stationarity of the parallel flow energy is used as a proxy; typically the mean of a sample should be at least two orders of magnitude smaller than the standard deviation — see Ref. [17] for details of this and of mode structure diagnostics. The principal scalings are those with respect to beta and collisionality, which follow nT/B^2 and n/T^2; that is, n and T in the edge operational diagram (cf. Ref. [18]). In an experiment these vary at constant B, not $\rho_s/L_\perp$, so it is important to note the effect of the gyro-Bohm flux velocity normalisation in terms of $c_s\rho_s^2/L_\perp^2$. This scales as $(\beta_e/C)^{1/2}$ in scans varying n and T holding all other parameters fixed.

The scan of full flux surface turbulence versus beta is presented herein. The base case is given by $n_e = 2\times10^{19}\,\mathrm{m}^{-3}$ and $T_e = T_i = 100\,\mathrm{eV}$ and $B = 2.5\,\mathrm{T}$ and $R = 3.3a = 1.65\,\mathrm{m}$ and $q = 3.5$ and $S = 2$ at $r_a = 0.965$. Nominal profiles are such that $L_T = L_n/2 = L_\perp = 0.035\,\mathrm{m}$, giving normalised local parameters of $\hat\beta = 1.75$ and $\hat\mu = 7.41$ and $C = 3.11$ and $\omega_B = 0.0424$ giving inductivity $\beta_e(qR/L_\perp)^2$, thermal nonadiabaticity $(m_e/M_D)(qR/L_\perp)^2$, collisionality $0.51(\nu_e L_\perp/c_s)\hat\mu$ and toroidal curvature forcing $2L_\perp/R$, respectively.

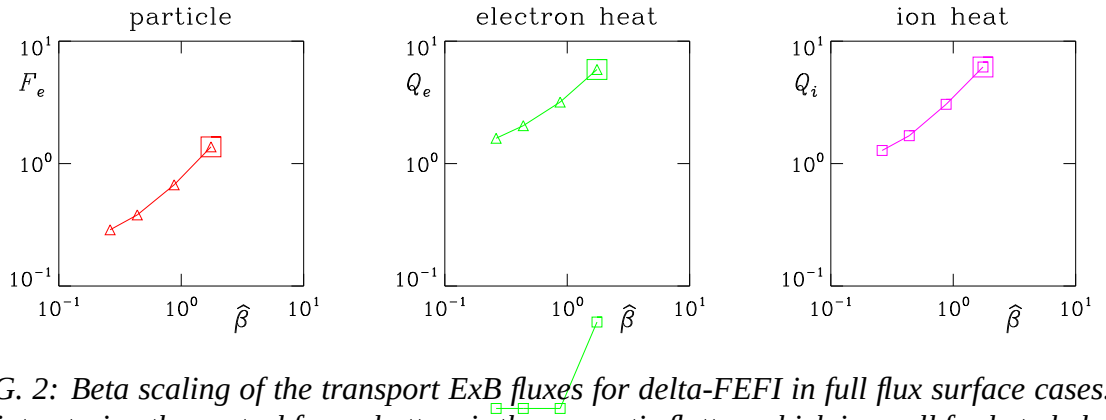

FIG. 2: Beta scaling of the transport ExB fluxes for delta-FEFI in full flux surface cases. The point entering the central frame bottom is the magnetic flutter, which is small for beta below the MHD regime. The trend is similar to fluid and gyrofluid cases with ion and electron temperature gradients.

The computational grid is $64 \times 1024 \times 32$ in $\{xys\}$ and 32×16 in $\{zw\}$ on a domain of $62.8\rho_s \times 1499\rho_s \times 2\pi qR$ and $-5 < z/V < 5$ and $0 < wB_0/T < 10$ respectively. Fluxtube boundary conditions are as described in Ref. [14]; it is important to note that periodic conditions in x are very damaging due to the admittance of an unphysical radial flow jet with $k_x = 0$. Dirichlet boundaries are used in $\{zw\}$ except at $w = 0$ where Neumann boundaries are used. The time step is $0.01L_\perp/c_s$. The numerical scheme is set up as in previous fluid and gyrofluid models [19,12]. The brackets use the 4th order Arakawa method [20], the $\mathcal{K}$ terms 4th order central differencing, the collisions use the 2nd order finite volume method, and the time step is the 3rd order step from Karniadakis [21]. Additional spatial hyperviscosity applied to (δf) is applied as in Ref. [12]; the delta-f gyrofluid moment variables are understood as a representation for (δf) following the derivation path in Ref. [11].

The basic transport scaling (ExB fluxes for particles and electron and ion energy with the magnetic flutter flux for electron energy) is given in Fig. 2. The result is unremarkable, serving only to confirm previous experience with fluid and gyrofluid models with ion and electron temperature gradients [22,23]. Cases with $\hat{\beta} > 2$ have so far led to very strong dynamics which eventually crash the runs; saturated states in this MHD-dominated regime are not yet available. With a complete gyrokinetic model covering the entire flux surface the result remains incompatible with the observed tokamak L-H transition. The H-mode [24,25] remains unexplained despite many claims over the past 20 years. The relevant transition data are given in the L-H transition region of the edge operational diagram [18], which the runs for T up to 150 eV have been able to cover.

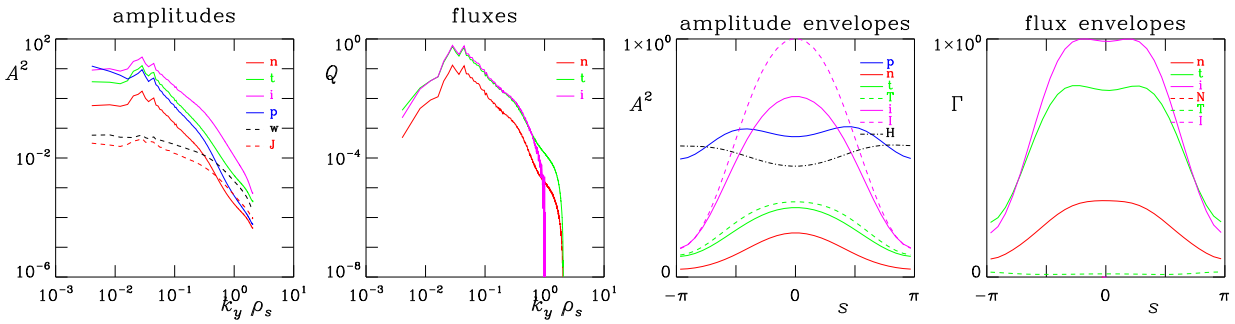

FIG. 3: Mode structure for delta-FEFI in full flux surface cases. State variable amplitude spectra peak in the MHD range ($k_y\rho_s < 0.1$) while current and vorticity are much flatter. The fluxes also peak for k_y much lower the linear growth peak at $k_y\rho_s \sim 0.15$. The geodesic resonance is at 0.06 (see text). The ballooning structure of amplitudes and fluxes is similar to gyrofluid experience [26,16].

The most interesting result in these cases so far is the strength of the mesoscale MHD regime shown by the saturated spectra. Drift-angle spectra and parallel envelopes in the nominal case are shown in Fig. 3. Short linear runs with initial amplitude set to 10^{-10} rather than 1.0 find the strongest growth close to $k_y\rho_s = 0.15$, already rather long-wave in the drift wave sense; this results from the large value $R/L_T = 47$ which causes $\hat{\mu}$ well larger than unity hence nonadiabatic thermal electrons. The nonlinear energy transfer [10] shows strong drive of the MHD range due to ExB vorticity advection. The above-unity values of both $\hat{\beta}$ and $\hat{\mu}$ lead to weak damping of the MHD shear-Alfvén component, allowing eddies in this range to persist long enough to enhance the gradient drive. Since the drift wave spectrum is held together by simultaneous coexistence of cascade/transfer to larger scale by vorticity advection and to smaller scale by ExB density/pressure advection [27–29], the energy balance at any wavelength has a nonlinear

input as well as an output. Since the rate of nonlinear transfer is larger than linear growth rates everywhere in the spectrum, the overall result does not depend on linear physics. Indeed, in Ref. [10] the transport scaling was to diverge completely from the linear growth rate result. From the point of view of experimental observations, large scale fluctuation ($> 1\,\mathrm{cm}$) and Bohm-like global scaling have been reported, and fluid computations have had difficulty reproducing this. The kinetic cases differ mainly due to the large trapped fraction in the electrons. The ExB heat flux peak is isotropic in energy (in $\{zw\}$) at a velocity roughly $2V_e$ and a peak is visible at $v_{\|} = 0$ and $\mu B_0/T_e = 2.5$; while the thermal ν_* is roughly 13 the kinetic one at $2V_e$ is 16 times less or about 0.8, which is low enough to matter. The dFEFI result produces more longwave activity than the GEM result for the same case (cf. Ref. [10]). The trapping effect on electrons may explain the large scale fluctuation observations.

Results on other topics such as sensitivity to ExB shear and zonal flow energetics [26,30] cannot be shown for space reasons. These will be reported at the IAEA FEC 2010 and published elsewhere.

3. Edge Turbulence Gyrofluid Studies

The following studies were done with global gyrofluid computations using the GEMR model: an ELM crash scenario involving ideal MHD ballooning destabilisation in Ref. [31], which gives a complete description of the model, a quantitative comparison with scrape-off layer turbulence in Ref. [32], integration with a full-wave Maxwell solver for simulated reflectometry suitable for quantitative experimental comparisons in Ref. [33]. In addition, a conformal coordinate system was derived to minimise coordinate deformation in shaped geometry while retaining all advantages of field alignment was given in Ref. [34].

References

[1] SUGAMA, H., Phys. Plasmas **7** (2000) 466.
[2] BRIZARD, A., Phys. Plasmas **7** (2000) 4816.
[3] BRIZARD, A. et al., Rev. Mod. Phys. **79** (2007) 421.
[4] MIYATO, N. et al., J. Phys. Soc. Japan **78** (2009) 104501.
[5] DUBIN, D. H. E. et al., Phys. Fluids **26** (1983) 3524.
[6] HAHM, T. S., Phys. Fluids **31** (1988) 2670.
[7] BRIZARD, A., Phys. Plasmas **2** (1995) 459.
[8] HAHM, T. S., Phys. Plasmas **3** (1996) 4658.
[9] SCOTT, B. et al., Phys. Plasmas **17** (2010) in press, arXiv:1008.1244.
[10] SCOTT, B. et al., Contrib. Plasma Phys. **50** (2010) 228.
[11] SCOTT, B., Phys. Plasmas **17** (2010) accepted, arXiv:0710.4899.
[12] SCOTT, B., Phys. Plasmas **12** (2005) 102307.
[13] SCOTT, B., Phys. Plasmas **5** (1998) 2334.
[14] SCOTT, B., Phys. Plasmas **8** (2001) 447.
[15] SCOTT, B., Plasma Phys. Contr. Fusion **45** (2003) A385.
[16] SCOTT, B., Contrib. Plasma Phys. **46** (2006) 714.
[17] SCOTT, B., Plasma Phys. Contr. Fusion **39** (1997) 1635.
[18] SUTTROP, W. et al., Plasma Phys. Contr. Fusion **39** (1997) 2051.
[19] NAULIN, V., Phys. Plasmas **10** (2003) 4016.
[20] ARAKAWA, A., J. Comput. Phys. **1** (1966) 119, Repr. vol 135 (1997) 103.
[21] KARNIADAKIS, G. E. et al., J. Comput. Phys. **97** (1991) 414.
[22] SCOTT, B., New J. Phys. **4** (2002) 52.
[23] SCOTT, B., Plasma Phys. Contr. Fusion **49** (2007) S25.
[24] WAGNER, F. et al., Phys. Rev. Lett. **49** (1982) 1408.
[25] GOHIL, P. et al., Nucl. Fusion **34** (1994) 1057.
[26] SCOTT, B., Phys. Plasmas **7** (2000) 1845.
[27] SCOTT, B., Phys. Fluids B **3** (1991) 51.
[28] SCOTT, B., Phys. Fluids B **4** (1992) 2468.
[29] CAMARGO, S. et al., **2** (1995) 48.
[30] SCOTT, B., Plasma Phys. Contr. Fusion **48** (2006) B277.
[31] KENDL, A. et al., Phys. Plasmas **17** (2010) 072302.
[32] ZWEBEN, S. J. et al., Phys. Plasmas **16** (2009) 082505.
[33] DA SILVA, F. et al., Development of a 2d full-wave je-fdtd maxwell x-mode code for reflectometry simulation, in *Proc. IRW9, Lisbon, 4-6 May*, 2009.
[34] RIBEIRO, T. et al., IEEE Transactions on Plasma Science **38** (2010) 2159.